Chemistry–A European Journal
Full Paper
doi.org/10.1002/chem.202004660
Chemistry Europe
European Chemical Societies Publishing

Transition Metal Reactivity | *Hot Paper*

Reactivity of Single Transition Metal Atoms on a Hydroxylated Amorphous Silica Surface: A Periodic Conceptual DFT Investigation

Xavier Deraet,[a] Jan Turek,[a] Mercedes Alonso,[a] Frederik Tielens,[a] Stefaan Cottenier,[b, c] Paul W. Ayers,[d] Bert M. Weckhuysen,[e] and Frank De Proft*[a]

Abstract: The drive to develop maximal atom-efficient catalysts coupled to the continuous striving for more sustainable reactions has led to an ever-increasing interest in single-atom catalysis. Based on a periodic conceptual density functional theory (cDFT) approach, fundamental insights into the reactivity and adsorption of single late transition metal atoms supported on a fully hydroxylated amorphous silica surface have been acquired. In particular, this investigation revealed that the influence of van der Waals dispersion forces is especially significant for a silver (98%) or gold (78%) atom, whereas the oxophilicity of the Group 8–10 transition metals plays a major role in the interaction strength of these atoms on the irreducible SiO_2 support. The adsorption energies for the less-electronegative row 4 elements (Fe, Co, Ni) ranged from −1.40 to −1.92 eV, whereas for the heavier row 5 and 6 metals, with the exception of Pd, these values are between −2.20 and −2.92 eV. The deviating behavior of Pd can be attributed to a fully filled d-shell and, hence, the absence of the hybridization effects. Through a systematic analysis of cDFT descriptors determined by using three different theoretical schemes, the Fermi weighted density of states approach was identified as the most suitable for describing the reactivity of the studied systems. The main advantage of this scheme is the fact that it is not influenced by fictitious Coulomb interactions between successive, charged reciprocal cells. Moreover, the contribution of the energy levels to the reactivity is simultaneously scaled based on their position relative to the Fermi level. Finally, the obtained Fermi weighted density of states reactivity trends show a good agreement with the chemical characteristics of the investigated metal atoms as well as the experimental data.

Introduction

Several decades of intensive scientific research have contributed to the emergence of d-metal-based catalysts as one of the most important workhorses for the synthesis of bulk chemicals, the development of fuel cells and the production of energy. However, the recent drive to develop more sustainable catalytic pathways has stimulated a growing interest for the progressive reduction in size of metal clusters to the most extreme situation of a single-atom catalyst (SAC).[1] A SAC is defined as a catalyst which only consists of isolated single atoms dispersed on a support, where neither spatial ordering nor interactions between the individual atoms can be observed.[1b] In addition, the individual metal atom must always provide the catalytic activity, to which nearby atoms or functional groups at the support might also contribute. Furthermore, the various catalytic sites of a SAC can show a different activity depending on the presence or absence of different interactions between the metal and the support.[1,2]

Despite the growing experimental[3–8] and computational[9–17] interest in SACs, challenges related to the lifespan and activity of this novel class of catalysts with respect to cluster-type catalysts still exist within the scientific community. The main concerns are usually associated with the concept of strong metal-support interactions (SMSI).[2] Consequently, an important part in the production of SAC consists of carefully selecting supports that minimize atom mobility, while offering highly stable active sites.[1] A prominent example of a support showing no

[a] X. Deraet, Dr. J. Turek, Prof. M. Alonso, Prof. F. Tielens, Prof. F. De Proft
Department of General Chemistry (ALGC), Vrije Universiteit Brussel (VUB)
Pleinlaan 2, 1050 Elsene, Brussels (Belgium)
E-mail: fdeprof@vub.be
[b] Prof. S. Cottenier
Department of Electrical Energy, Metals
Mechanical Constructions and Systems
Ghent University
Technologiepark 46, 9052 Zwijnaarde (Belgium)
[c] Prof. S. Cottenier
Center for Molecular Modeling, Ghent University
Technologiepark 46, 9052 Zwijnaarde (Belgium)
[d] Prof. P. W. Ayers
Department of Chemistry and Chemical Biology, McMaster University
Hamilton, Ontario L8S 4M1 (Canada)
[e] Prof. B. M. Weckhuysen
Inorganic Chemistry and Catalysis Group
Debye Institute for Nanomaterials Science, Utrecht University
Universiteitsweg 99, 3584 CG Utrecht (The Netherlands)
Supporting information and ORCIDs from the authors for this article are available on the WWW under:
https://doi.org/10.1002/chem.202004660.

strong metal-support interactions is amorphous silica. In addition to its irreducible character, silica is a thermally stable support with very convenient mechanical properties making it very suitable for catalytic and technological purposes.[18] Thus, catalysts consisting of d-transition metals on a silica support are used in a plethora of chemical reactions.[19]

Although the increasing computational relevance of this new type of catalyst seems to be reflected in the recent literature,[9–17] systematic ab initio studies of SAC effects appear to be much less extensively described as compared to single atom catalytic mechanistic studies. From the current literature it can nonetheless be concluded that the strength by which these transition metal atoms adsorb on the surface is strongly driven by the above-mentioned concept of SMSI. Accordingly, the adsorption of d-transition metal atoms on defect-free irreducible oxide supports (MgO,[20] SiO_2[21] and Al_2O_3[22]) will often be accompanied by less pronounced interactions than in the case of SMSI surfaces like TiO_2[23] and CeO_2.[24] While the metal-support interactions in the non-SMSI state often depend on a combination of effects such as van der Waals dispersion, polarization and sometimes orbital mixing,[20–21] the reducible character of TiO_2 and CeO_2 turns out to play a crucial role in the observed enhanced adsorption.[22,24] This reducible character facilitates a more pronounced charge transfer from the metal to the surface which enables the formed d-metal cation to interact more strongly with the O^{2-} atoms of the surface in comparison to the neutral atom. Notwithstanding the diverse nature of the interactions, it appears that regardless of the type of support, the adsorption is usually accompanied by a changing electronic configuration of the metal.[20–24] This quenching of the spin moment is often related to the fact that upon formation of a bond between the metal and support, the outer *s*-electrons of the transition metal are promoted into the incomplete d-shell in order to reduce the number of unpaired electrons.

The presented work is focused on the adsorption of single late transition metal atoms on a hydroxylated amorphous silica surface. The reactivity of the resulting supported single atom catalysts was elucidated using conceptual DFT (cDFT) indices. These descriptors have already been extensively used to assess the reactivity of molecules regarding hard and soft reagents[25] but are significantly less applied in the field of solid-state chemistry. We are, however, convinced that the use of these indices as predictive tools can be of major interest for the description of experimental catalytic findings. For instance, the systematic probing of cDFT descriptors enables the assessment of possible trends in reactivity between similar systems, which might contribute to a more concept-oriented development of catalysts. These indices also provide an overall picture of the different sites of a surface that are most likely to interact through either charge transfer (soft systems) or electrostatic interactions (hard systems). Furthermore, insight into the intrinsic reactivity (i.e., orbital- or electrostatically oriented reactivity) of the catalytic particle can be obtained without the need for prior modelling of interactions with external reagents. Consequently, an important part of this paper consists of evaluating the performance of three existing approaches (finite difference approximation, density of states integration and Fermi weighted density of states integration) in determining accurate reactivity indices for these periodic systems.

Computational Methods

The adsorption and chemical reactivity of single d-transition metal atoms of Groups 8–11 on a previously constructed amorphous silica surface[26] were investigated by means of periodic, spin-polarized density functional theory (DFT) calculations with the Vienna Ab Initio Simulation Package[27] (VASP 5.4.4). The fully hydroxylated plain silica surface model with unit cell dimensions of $a=12.77$ Å, $b=17.64$ Å and $c=25.17$ Å (vacuum layer of 15 Å) was optimized with the generalized gradient approximated PBE functional[28] including the Grimme DFT-D3 empirical dispersion with the Becke-Johnson (BJ) damping function.[29] This correction was included in order to take into account the effects of non-covalent interactions on the binding of a single d-transition metal atom with the silica support. The surface consists of 27 SiO_2 units with 13 terminating hydroxy groups, which corresponds to a hydroxy density of 5.8 OH^- nm^{-2}. The interactions between the explicitly treated valence electrons and the ionic cores were described using the projector-augmented-wave method (PAW),[30] in which the wave functions were expanded up to a kinetic energy of 400 eV. Considering the large size of the supercell, all calculations, unless otherwise stated, were executed considering the Γ-point only, and the partial occupancies for each wave function are set using the Gaussian smearing method with a smearing width of 0.001 eV.

Each model representing the adsorption of a single transition metal atom on the hydroxylated amorphous SiO_2 surface was fully optimized (i.e., full relaxation of the ionic positions) with a convergence criterion for the energy of 10^{-6} eV. The adsorption energy was calculated from Equation (1) with *E*(*M*), *E*(*S*) and *E*(*M/S*) representing the energy of the free metal atom, plain silica surface and adsorbed metal atom on silica, respectively. The Γ-point only calculations on a free single transition metal atom were performed in a nearly cubic periodic box. In order to confirm the convergence of the obtained energy values for the single atoms, these calculations were repeated with both a (2×2×2) and (4×4×4) Γ-centered Monkhorst-Pack[31] k-point grid. These k-space convergence data can be found in Table S1 (Supporting Information) and reveal that an increase in considered amount of k-points only affects the energy of the atom with an order of magnitude of 10^{-6} eV. [Eq. (1)]

$$E_{ads} = E(M/S) - E(M) - E(S) \quad (1)$$

By analogy with the work of Schlexer and Pacchioni on the adsorption and dimerization of late transition metals on various quartz surfaces,[21] we evaluated the total contribution of the dispersion into the adsorption energy by means of Equation (2), in which V_{DISP} represents the amount of vdW dispersion included in the total electronic energy of the respective system.

$$\%_{DISP}(M/S) = \frac{[V_{DISP}(M/S) - V_{DISP}(M) - V_{DISP}(S)]}{E_{ads}} \quad (2)$$

The corresponding atomic charges were obtained using the Bader decomposition scheme[32] and converted into net charges by taking the difference between the number of valence electrons (*Z*) and the charge obtained from the decomposition scheme (q_{Bader}), as indicated in Equation (3). The energies and charge densities of the $N+1$ and $N-1$ electron systems were generated by performing

one full ionic cycle without ionic movement on the already optimized *N*-electron geometry. The exact number of electrons to be considered for each system was entered manually using the NELECT keyword in VASP.

$$q_{net} = Z - q_{Bader} \tag{3}$$

Besides charge analysis, the nature of the interactions between the surface and the transition metal atom was investigated using the density of states (DOS) of the *N*-electron systems at the energetically most favored binding site. These plots were evaluated over 3000 energy grid points and a (15×15×1) Γ-centered Monkhorst-Pack k-point grid, starting from the previously generated charge density at the Γ-point only.

Reactivity indices: Conceptual reactivity indices, obtained from a Taylor series expansion containing *n*th-order derivatives of the energy functional [Eq. (4)], represent the response of a system to small perturbations in the number of electrons *N* and/or the external potential $v(\vec{r})$.[33,34]

$$\Delta E = \left(\frac{\partial E}{\partial N}\right)_{v(\vec{r})}\Delta N + \int\left(\frac{\delta E}{\delta v(\vec{r})}\right)_{N}\Delta v(\vec{r})d\vec{r} + \frac{1}{2}\left(\frac{\partial^2 E}{\partial N^2}\right)_{v(\vec{r})}\Delta N^2 + \int\frac{\partial\delta E}{\partial N\delta v(\vec{r})}\Delta N\Delta v(\vec{r})d\vec{r} + \int\frac{\partial^2\delta E}{\partial N^2\delta v(\vec{r})}\Delta N^2\Delta v(\vec{r})d\vec{r} + \tag{4}$$

In this Taylor expansion, the first- and second-order derivatives of the energy with respect to *N* correspond to the electronic chemical potential (μ)[35] and chemical hardness (η).[36] Within the quadratic energy model,[36,37] which is known to exactly reproduce the normalization conditions of the electron density and its derivatives,[38] the electronic chemical potential and chemical hardness can be written in terms of the ionization potential (*I*) and the electron affinity (*A*), as can be inferred from Equations (5) and (6). Accordingly, the chemical potential is given as the negative value of the average of *I* and *A* or the electronegativity (χ).[35] Besides, the chemical hardness, defining the reluctance of the system towards charge transfer, is obtained as a difference between *I* and *A* or as the inverse of the chemical softness (*S*).[36]

$$\mu = \left(\frac{\partial E}{\partial N}\right)_{v(\vec{r})} = -\chi \approx -\frac{I+A}{2} \tag{5}$$

$$\eta = \left(\frac{\partial^2 E}{\partial N^2}\right)_{v(\vec{r})} = I - A = \frac{1}{S} \tag{6}$$

These quantities are constant over space and characterize the overall global chemical response of the system of interest towards an electron transfer. By contrast, derivatives with respect to the external potential and mixed derivatives appear to vary with respect to $\vec{r}$. Consequently, these local descriptors resolve the chemical reactivity of specific locations within the system.

The first mixed derivative, defined as the Fukui function [$f(\vec{r})$], describes the response of the system when applying simultaneous perturbations in the number of electrons and external potential.[39] Due to the discontinuity of the electron density with respect to the number of electrons,[40] the Fukui function has to be split into a right-handed and a left-handed derivative. Within the finite difference approach, these right [$f^+(\vec{r})$] and left [$f^-(\vec{r})$] derivatives describe systems to which an electron is added or from which an electron is removed, respectively, and are approximated as the difference between the electron densities of the *N* and *N*+1 or *N*−1 electron systems [Eq. (7)].[39] The obtained isosurfaces for $f^-(\vec{r})$ and $f^+(\vec{r})$ highlight regions that are prone, respectively, to electrophilic or nucleophilic attacks of soft reagents. Alternatively, the dual descriptor [$f^2(\vec{r})$], evaluated as the difference between the electrophilic and nucleophilic Fukui function [Eq. (8)], provides a one-shot picture of the chemical reactivity of the surfaces highlighting simultaneously both nucleophilic and electrophilic regions.[41,42]

$$f^+(\vec{r}) = \left(\frac{\partial\delta E}{\partial N\delta v(\vec{r})}\right)^+ = \rho_{N+1}(\vec{r}) - \rho_N(\vec{r})$$
$$f^-(\vec{r}) = \left(\frac{\partial\delta E}{\partial N\delta v(\vec{r})}\right)^- = \rho_N(\vec{r}) - \rho_{N-1}(\vec{r}) \tag{7}$$

$$f^2(\vec{r}) = \left(\frac{\partial^2\delta E}{\partial N^2\delta v(\vec{r})}\right) = f^+(\vec{r}) - f^-(\vec{r}) \tag{8}$$

A final way to probe the reactivity towards soft reagents consists of determining the local softness [$s(\vec{r})$], which is defined within the finite difference approach as the product of the global chemical softness (*S*) and the Fukui function of interest.[43] Consequently, the local softness can be evaluated for system in which electrons are added [$s^+(\vec{r})$] or removed [$s^-(\vec{r})$] by using Equation (9).

$$s(\vec{r}) = Sf(\vec{r}) \tag{9}$$

Besides, it was shown by Yang and Parr that for periodic (metallic) systems the local softness is related to the local density of states (LDOS) at the Fermi level.[43] Based on this insight, another method involving the integration of the total ($g(\varepsilon)$) and local ($g(\varepsilon, \vec{r})$) density of states over the smallest possible range of the chemical potential μ was introduced for the local softness [Eq. (10)].[44] This approach has been extensively applied in the studies of zeolites,[45] nanotubes,[46] silicon surfaces[47] and alkaline earth oxides.[48]

$$s(\vec{r}) = \frac{\lim_{\delta\mu\to 0}\left(\frac{1}{\delta\mu}\right)\int_{\mu}^{\mu+\delta\mu} g(\varepsilon,\ \vec{r})\mathrm{d}\varepsilon}{\lim_{\delta\mu\to 0}\left(\frac{1}{\delta\mu}\right)\int_{\mu}^{\mu+\delta\mu} g(\varepsilon)\mathrm{d}\varepsilon}S \tag{10}$$

An alternative formulation that takes into account the variable contribution of an energy state to the final reactivity depending on its location with respect to the Fermi level was proposed by Zhuang and co-workers in both a global and local form.[49] The obtained Fermi softness quantifies the global (S_F) or local (s_F) reactivity of the considered system as a summation over a suitable energy range of the product of a weight function and the total or local density of states [Eq. (11)]. The spreading of this function, defined as the derivative of the Fermi–Dirac distribution function, is determined by the nominal electron temperature (k_BT) and peaks around the Fermi level. As shown in the Appendix, the Fermi softness appears to be a good estimate of *S* if one assumes that the DOS varies only slowly with μ and hence corresponding relaxation terms can be neglected.

$$S_F = \int_{-\infty}^{+\infty} g(\varepsilon)\left(\frac{\partial f(\varepsilon)}{\partial \mu}\right)_v \mathrm{d}\varepsilon$$

$$s_F(\vec{r}) = \int_{\mu\pm\delta\mu}^{\mu} g(\varepsilon,\vec{r})\left(\frac{\partial f(\varepsilon)}{\partial \mu}\right)_v \mathrm{d}\varepsilon \qquad (11)$$

Results and Discussion

Adsorption of SACs on amorphous silica support

Before assessing the chemical reactivity on the basis of conceptual DFT indices, we have first characterized the adsorption of single d-transition metal atoms from Group 8 (Fe, Ru and Os), Group 9 (Co, Rh and Ir), Group 10 (Ni, Pd and Pt) and Group 11 (Cu, Ag and Au) on a hydroxylated amorphous silica surface. In order to find the most stable adsorption pattern for each transition metal atom, five well-defined binding sites (indicated as T_1 to T_5) were investigated. As depicted in Figure 1, the binding sites T_1 and T_5 represent silica ring systems containing five Si atoms, while ring systems consisting of six Si atoms are denoted as T_3 and T_4 sites. Furthermore, it can be observed that all sites are characterized by a different number of hydroxy groups. Besides, we quantified the adsorption strength of the single metal atom on a smaller ring system consisting of four Si atoms (T_2). In view of the number of considered metal atoms as well as the complexity of the amorphous silica surface in comparison to the crystalline supports, this study does not involve any alternative binding sites induced by the presence of defects such as oxygen vacancies, Si-O$^{\bullet}$ radicals, Si^{3+} and Si^{5+} sites. Similarly, a plausible reactivity of the silanol groups yielding direct Si-O-M bonds, which were recently shown to play a role in analogous systems,[50] is not within the scope of this study.

Table 1. Overview of the PBE-D3BJ adsorption energies for all investigated single metal atoms at five different binding sites of the amorphous silica surface, as described in Figure 1. The values marked in bold are corresponding to the energetically most favored binding site.

	E_{ads} [eV]				
	T_1	T_2	T_3	T_4	T_5
Fe	−1.04	−0.98	−1.19	−0.57	**−1.40**
Ru	**−2.40**	−1.73	−2.15	−1.43	−2.31
Os	−2.23	−2.05	−2.41	−1.64	**−2.58**
Co	−1.46	−1.36	−1.50	−0.98	**−1.78**
Rh	−2.00	−1.72	−1.94	−1.30	**−2.20**
Ir	−2.60	−2.41	−2.87	−1.79	**−2.92**
Ni	−1.70	−1.61	−1.67	−1.27	**−1.92**
Pd	**−1.21**	−0.83	−1.10	−1.10	−1.10
Pt	−2.56	−2.31	−2.38	−1.76	**−2.62**
Cu	**−0.78**	−0.63	−0.10	−0.60	−0.42
Ag	−0.29	0.62	0.91	**−0.37**	0.02
Au	−0.31	0.16	−0.18	−0.39	**−0.49**

The adsorption energies of the metals at the selected binding sites (Figure 1) are summarized in Table 1. From this table it can be established that the adsorption energy is highly dependent on the investigated metal. As expected, the weakest adsorption energies for the most stable geometries, which vary from −0.78 (Cu) to −0.37 eV (Ag) are obtained for the inert Group 11 metal atoms. The fourth period elements (Fe, Co and Ni) as well as Pd are characterized by intermediate adsorption energies ranging from −1.21 (Pd) to −1.92 eV (Ni). The remaining metal atoms belonging to the fifth and sixth period appear to interact very strongly ($E_{ads} > -2.00$ eV) with the silica support with a maximum adsorption energy of −2.92 eV for a single Ir atom. Very similar energetic trends were noticed in a study on the adsorption of single d-transition metals on hydroxylated quartz surfaces by Schlexer and Pacchioni.[21] For instance, very low adsorption energies fluctu-

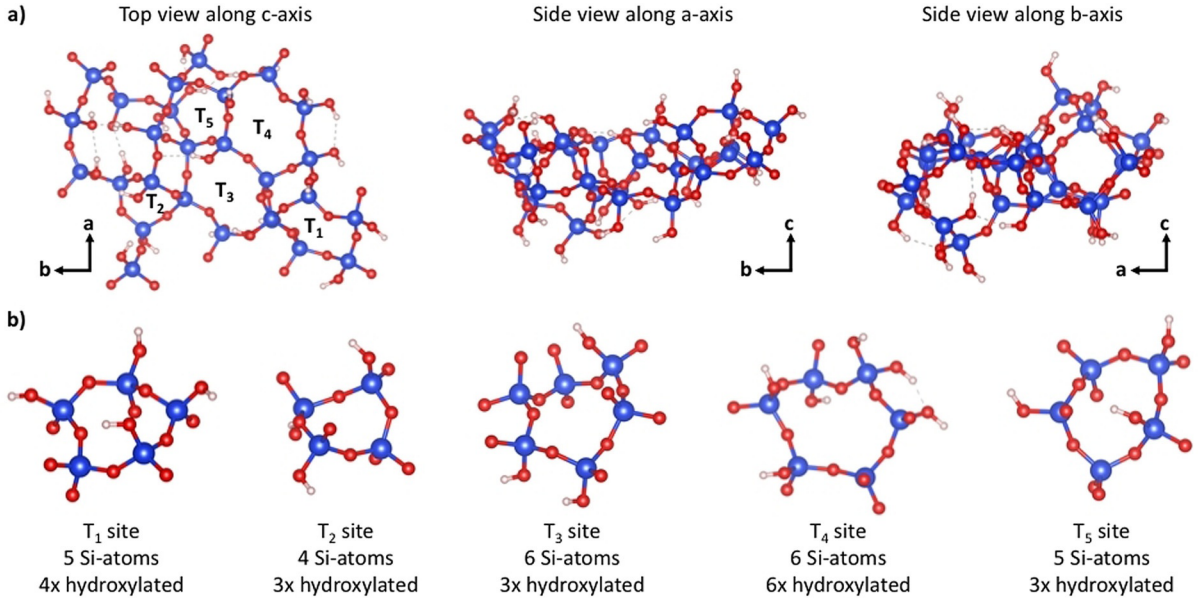

Figure 1. a) General overview of the unit cell of the hydroxylated amorphous silica surface model. b) Top view detail of the five binding sites on which the adsorption of Group 8–11 single d-transition metal atoms was investigated.

ating around −0.30 eV were obtained for Group 11 metals (Cu, Ag and Au), while the heavier Rh (−1.53 eV) and Pt (−1.51 eV) systems were characterized by the highest values.[21] However, in contrast to our study, the adsorption of Ir was considerably weaker on their quartz surface as an adsorption energy of only −0.97 eV was obtained.[21] The generally higher adsorption energies in our investigation can probably be attributed to the increased flexibility of the amorphous silica surface as compared to the rather rigid crystal lattice of quartz, hence giving rise to shorter bonding distances between the oxygen atoms of the amorphous surface and the transition metal atom. On the quartz surface, the shortest distance between the iridium atom and an oxygen atom corresponds to 2.28 Å,[21] whereas on the amorphous silica surface this is reduced to only 1.94 Å. Additionally, the alternative approach to treat the dispersion corrections may also partially explain the observed differences.

Furthermore, it was also observed that our computed adsorption energies are reasonably similar to the values described in the literature for the adsorption of SAC on the irreducible alumina (Al_2O_3) surface,[22a,b,51] but significantly weaker than those found for the reducible rutile (TiO_2) support.[23] As such, the adsorption of a single Pd, Pt or Cu atom on the α-Al_2O_3 support is, respectively associated with an energy of −1.35, −2.20 and −0.70 eV,[22a,b,51] whereas our calculations on the amorphous silica surface give rise to values of −1.21, −2.62 and −0.78 eV. In contrast, the magnitude of the energies for the adsorption of the row 4 elements (Fe, Co, Ni) on the irreducible silica surface is much smaller, by at least a factor of two, with respect to the values for the reducible rutile support exhibiting strong metal-support interactions. Accordingly, the adsorption of a single Fe, Co or Ni atom on the latter support is characterized by adsorption energies ranging between −3.50 and −3.32 eV,[23] while for amorphous silica values fluctuating between −1.92 and −1.40 eV are observed. The strong analogies between the adsorption energies for the alumina and silica support can hence be considered as a first indication of the fact that the amorphous silica surface retains its irreducible character upon adsorption of the SAC.

Despite the pronounced differences in adsorption energies between the different silica-supported metals, a clear preference emerges for the T_5 binding site and, to a lesser extent, for the T_1 and T_3 sites, irrespective of the metal. Details of the optimized geometries representing the adsorption of a single Ru and Ni atom on the T_1, T_3 and T_5 site of the amorphous silica surface are shown in Figure 2. For the remaining metal atoms, the representation at the most stable binding site can be found in Figure S1 (Supporting Information). From these structures, it can be concluded that the transition metal, regardless of the binding site, undergoes a double interaction with oxygen atoms that are either part of the cyclic SiO_2 moieties or from a silanol functionality, as it is the case for the T_1 site. During the geometry optimizations, the hydrogen atom belonging to the interacting silanol group rotates away from the transition metal, suggesting that the metal-oxygen interaction involves the lone pair of the oxygen atom. Besides, it should also be noted that these interactions are almost continuously associated with the disruption of the cyclic Si_5 (T_1 and T_5) or Si_6 system (T_3). Furthermore, it turns out that this ring opening is absent in the case of the energetically less advantageous T_4 and T_2 binding sites. For the T_2 binding site, the reduced adsorption energy can probably be attributed to the increased strain and steric hindrance associated with smaller ring systems. The large difference in adsorption energy between the T_3 and T_4 sites, which both correspond to a cyclic system consisting of six Si atoms surrounded by, respectively, 3 and 6 silanol groups, enables us to assume that the adsorption of transition metal atoms from Group 8–10, with the exception of Pd, is destabilized by an increasing degree of hydroxylation.

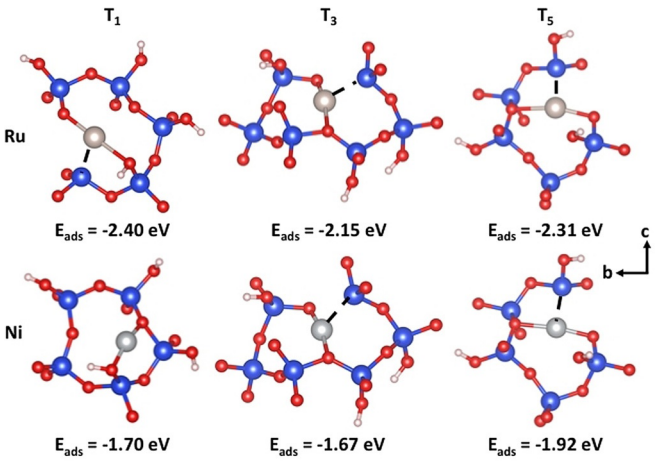

Figure 2. Top view of the optimized geometries representing the adsorption of a single Ru or Ni atom at the three energetically most favorable binding sites of a hydroxylated amorphous SiO_2 surface along with the corresponding adsorption energies.

The previous discussion seems, however, not to be applicable for the inert Group 11 transition metals, as the small adsorption energies are most probably positively influenced by a higher degree of hydroxylation. Consequently, the strongly hydroxylated T_4 site leads to the most stable configuration for silver and appears to be the second most advantageous site for adsorption of a gold or copper single atom on silica. Nevertheless, the distances between these metals and the silica surface are much larger than for the remaining metals. In addition, the adsorption energies for Ag and Au arise almost entirely from van der Waals dispersion forces (98 and 78%). The large contribution of van der Waals dispersion forces to the adsorption of these single metal atoms on hydroxylated defect-free quartz surfaces (115 and 84%) was also observed by Schlexer and Pacchioni.[21] Based on these facts, we hypothesize that silica supported Ag and Au are unsuitable for the development of stable single-atom catalysts.

A graphical representation of the adsorption energies at the most-favored binding site for all studied metals allowed us to establish that, with the exception of Pd, the adsorption strength of Group 8–10 metals tends to intensify as one moves down the group of the periodic table (Figure 3a). To discern these energetic trends, we focus on the difference in magnetic moment between the free ($|\mu_M|$) and adsorbed ($|\mu_{M/S}|$) metal atom as well as on density of states and Bader charge analysis. In order to avoid the general underestimation of the magnetic

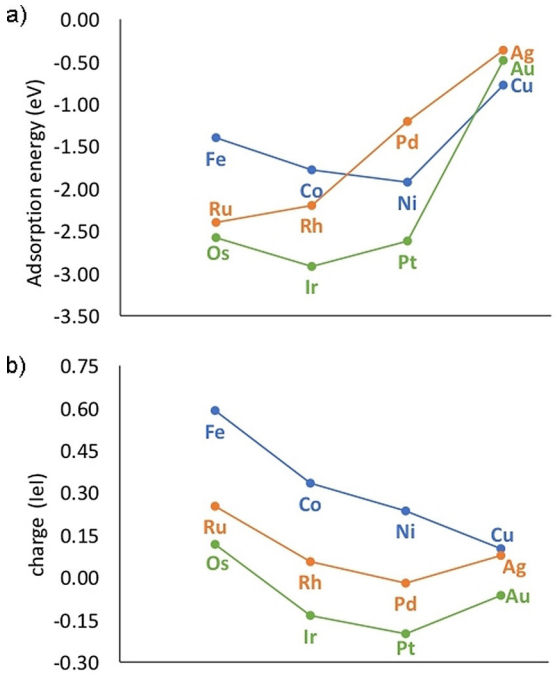

Figure 3. Graphical representation of the adsorption energies of the most stable geometries (a) and respective Bader charges (b) for the investigated d-transition metal atoms.

moment due to interstitial spaces related to the Wigner-Seitz spherical model,[52,53] the total magnetic moment determined over the entire volume of the unit cell was used. Since the considered plain silica surface does not contain any unpaired electron ($\mu = 0\ \mu_B$), differences in total magnetic moment upon adsorption can be fully attributed to the adsorbed d-transition metal. The obtained magnetic moments for the free d-transition metals ($|\mu_M|$) were compared with their ground state spin multiplicities as mentioned in literature.[54] All structural and electronic parameters used in the following discussion are summarized in Table 2.

The values of the magnetic moment show a clear connection between the low adsorption energy and the preservation of the magnetic moment for the Pd and inert Group 11 atoms, whereas for all systems characterized by medium and large adsorption energies the magnetic moment of the metal atom upon adsorption decreases by two. Accordingly, the coordination between the metal and the oxygen atoms of the silica surface induces a rearrangement of the atomic energy levels of the metal atom, changing its most stable spin state. More precisely, this quenching of the magnetic moment implies the formation of s–d hybrid orbitals and hence induces the promotion of the outer s-electrons of the transition metal into the incomplete d-shell. This effect was already described previously for other irreducible supports as well.[20] The presence of such a hybridization effect can, in addition to the change in magnetic moment, be also derived graphically from the local density of states (Figure 4 for the strongest interacting Ir metal). Consequently, Figure 4 clearly reveals that the contributions of the outer s-orbital of the transition metal are completely smeared over the different d-orbitals, which confirms the presence of hybrid orbitals. Furthermore, these orbitals also appear to interact to a given extent with the p-orbitals of the nearest oxygen and silicon atoms whose mutual bond is broken upon adsorption of the transition metal. However, in contrast to the oxygen atom with the shortest M–O distance (oxygen 1), the contribution of the p-orbitals of the second interacting oxygen atom (oxygen 2) does overlap to a much lesser extent with the d-orbitals of the metal and mainly coincides with the original valence band of the plain silica surface (Figure 4). This may indicate that the stabilization of the SAC upon adsorption on silica is associated with different types of interaction. These observations also apply to the other Group 8–10 systems, for which the total and local density of states can be found in Figures S2–S20 (Supporting Information).

To assess the nature of these metal-oxygen and metal-silicon interactions, we focused on the analysis of both the charge density and bonding distances. The isosurfaces for the region surrounding the transition metal are visualized in Figure 5. In

Table 2. Adsorption energies at the most favored binding site along with the magnetic moments, Bader charges, Mulliken electronegativity and relevant bonding distances.

	E_{ads} [a]	$\%_{DISP}$ [b]	$\lvert\mu_M\rvert$ [c]	$\lvert\mu_{M/S}\rvert$ [d]	q_M [e]	$\Delta\chi_M$ [f]	d_{M-O} [g]	Σ_{cov} (M–O)	d_{M-Si} [h]	Σ_{cov} (M–Si)
Fe	−1.40	28	4.00	2.00	0.59	3.48	1.83/2.05	1.98	2.24	2.43
Ru	−2.40	17	4.00	2.00	0.25	3.04	1.95/2.23	2.12	2.25	2.57
Os	−2.58	21	4.00	2.00	0.12	2.64	1.96/2.19	2.10	2.28	2.55
Co	−1.78	20	3.00	1.00	0.33	3.24	1.80/1.99	1.92	2.17	2.37
Rh	−2.20	17	3.00	1.00	0.06	3.24	1.98/2.21	2.08	2.25	2.53
Ir	−2.92	14	3.00	1.00	−0.14	2.14	1.94/2.14	2.07	2.25	2.52
Ni	−1.92	19	2.00	0.00	0.24	3.14	1.81/1.99	1.90	2.17	2.35
Pd	−1.21	27	0.00	0.00	−0.02	3.09	1.98/2.18	2.05	2.22	2.45
Pt	−2.62	18	2.00	0.00	−0.20	1.94	1.99/2.17	2.02	2.24	2.42
Cu	−0.78	29	1.00	1.00	0.10	3.06	2.03/3.23	1.98	3.24	2.43
Ag	−0.37	98	1.00	1.00	0.08	3.02	3.00/3.19	2.11	3.82	2.56
Au	−0.49	78	1.00	1.00	−0.06	1.77	2.21/3.18	2.02	2.32	2.47

[a] Adsorption energy [eV]. [b] Contribution of dispersion forces to the obtained adsorption energies [%]. [c] Magnetic moment of free metal atoms [μ_B]. [d] Magnetic moment of adsorbed metal atoms [μ_B]. [e] Net Bader charges of the metal atoms adsorbed on the silica support [$|e|$]. [f] Difference in Mulliken electronegativity between the free metal atom and oxygen atom[55] [eV]. [g] Metal–oxygen distances [Å]. [h] Metal–silicon distances [Å].

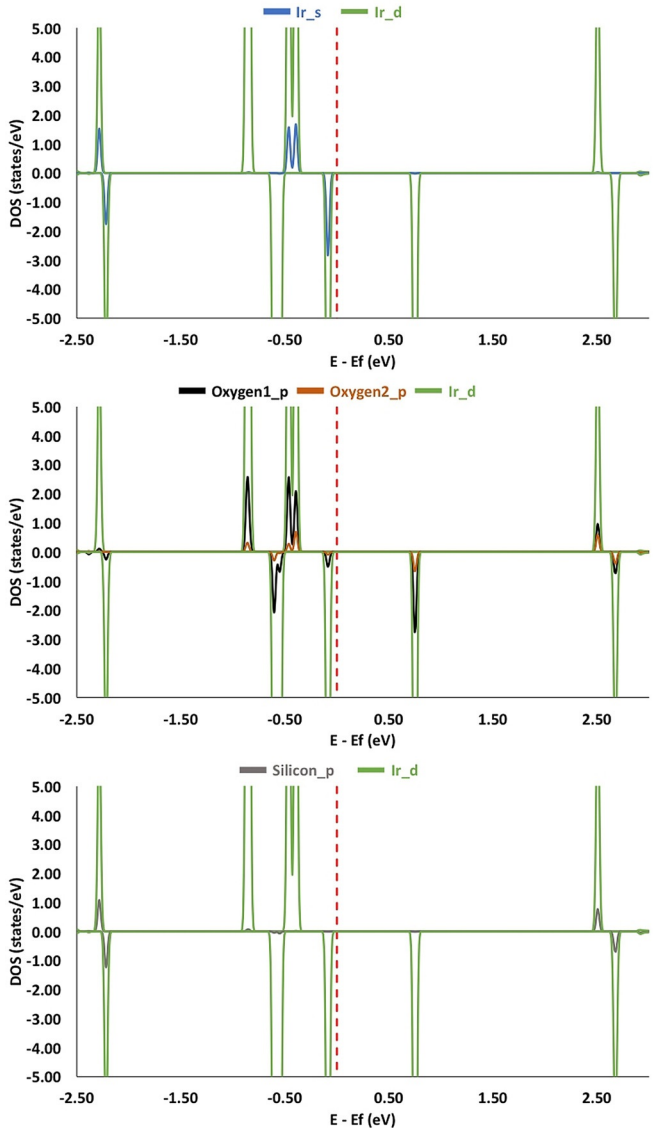

Figure 4. Local density of states (LDOS) of a single silica-adsorbed Ir atom projected onto s- and d-orbital contributions (top) as well as p-orbital contributions of the nearest oxygen atoms (middle) and silicon atom (bottom). The red dotted lines represent the Fermi level.

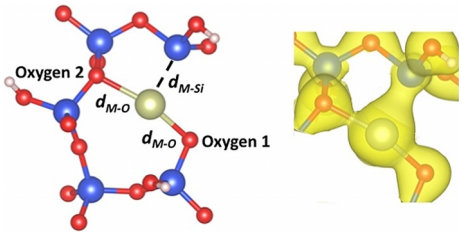

Figure 5. Left: Optimized geometry representing the adsorption of a single Ir atom at the energetically most favorable binding site with investigated bond lengths. Right: Isosurfaces representing the charge density occurring upon adsorption of a single Ir atom at an isovalue of 0.005 a.u visualized by means of the VESTA software.[57]

general, highly localized isosurfaces corresponding to a charge accumulation around atoms suggest the presence of an ionic interaction, whereas a fairly distributed charge density coincides with the sharing of electrons typical for a covalent interaction. Since no remarkable accumulation or depletion of charge at the level of neither the d-metal atom nor the oxygen and silicon atom is observed (Figure 5), but rather an equal dispersion of the charge density at the level of the metal-oxygen and metal-silicon bond, it can be hypothesized that these interactions have a significant covalent character. This is further supported by the length of the relevant metal-oxygen and metal-silicon bonds. Both M–Si and M–O bonds, which are formed upon breaking of the Si–O bond, are consistently shorter than the sum of the covalent radii of the respective atoms.[56] On the other hand, the second metal-oxygen bond is in all cases approximately 0.1 Å longer than the Σ_{cov}(M–O). This agrees well with the results obtained from the analysis of the local density of states, where only minor signals from the appropriate oxygen p-orbitals were found in the vicinity of the Fermi level. This suggests that this interaction is neither covalent nor ionic but can be best described as a rather strong donor-acceptor interaction between the lone pair of the oxygen and empty d-orbitals of the metal. As such, it can be hypothesized that the single metal atoms bind covalently to the silica surface upon breaking of the Si–O bond and formation of M–O and M–Si bonds, while an additional donor-acceptor interaction between the metal and the lone pair of the neighboring oxygen atom further stabilizes the formed catalytic complex.

Despite the presence of these covalent interactions, charge transfer between the metal atom and the support appears to be minimal. Furthermore, as graphically depicted in Figure 3b, the Bader charges show a decreasing behavior when moving down the groups and across the periods, with the exception of Ag and Au. This also demonstrates that the adsorption of the metal is not driven by the charge transfer process, as the elements with the strongest adsorption energy (rows 5 and 6) have the smallest Bader charge. The lack of charge transfer is more evidently observed when comparing the obtained Bader charges for the silica-supported row 4 elements with those obtained for the reducible TiO_2 surface. Accordingly, the adsorption of a single Fe, Co or Ni atom on the latter support gives rise to a charge transfer of 1.16, 1.01 and 0.95 $|e|$,[58] respectively, which corresponds to a two- to fourfold increase in charge transfer with respect to silica. Furthermore, the observed trends in Bader charges and adsorption energies seem to be closely related to the oxophilicity of the transition metal. The oxophilicity, describing the strength of the ionic character of the oxygen–metal bond and thus the charge transfer, appears to be strongly influenced by the difference in Mulliken electronegativity ($\Delta\chi_M$) between the transition metal and oxygen atom.[59] As shown in Table 2, the differences in electronegativity exhibit a decreasing trend when moving down the groups and across the periods by analogy with the Bader charges. Consequently, a decreasing $\Delta\chi_M$ implies a less distinct tendency to transfer electrons from the metal to the surface and hence a less pronounced metallic charge and oxophilic behavior. In this regard, the iron atom appears to be the most prone to charge transfer towards the oxygen atom ($q_{Fe} = 0.59$)

resulting in a stronger ionic character at the expense of the lowest adsorption energy, when excluding Pd. This suggests that the silica surface cannot easily accommodate this charge given its irreducible character. This observation combined with the fact that the calculated adsorption energies are less pronounced than in the case of the reducible TiO_2 support, but of the same order of magnitude as for Al_2O_3, allow us to conclude that the studied silica surface retains its electronic properties. This is further reinforced by the finding that the main orbital contribution around the Fermi level originates from the d-orbitals of the transition metals. Consequently, it can be concluded that the possible catalytic activity of the silica-supported single-atom catalyst should originate from the transition metal itself, while a limited number of covalent and noncovalent interactions ensure stabilization of this catalyst. This observation fits the definition of a SAC, in which it is stated that the active site must always contain the individual metal atom and eventually include additional functional groups or nearby atoms of the support. With the active site of the different SAC systems being clearly defined, we will now focus on describing the chemical reactivity of this site by means of conceptual reactivity indices. Given the weaker interaction between the amorphous silica surface and the inert Group 11 metals as well as the strong influence of van der Waals dispersion forces on their adsorption energies, it was decided to limit the subsequent conceptual reactivity study to the Group 8–10 systems.

Evaluating the reactivity of silica-supported SACs through a finite difference approach

The most commonly used approach to determine conceptual DFT indices relies on the finite difference approximation in which indices are described based on differences in vertical ionization potential or electron affinity and their associated electron densities. The global reactivity of the entire surface is described through the use of the Mulliken electronegativity (χ) and global softness (S). However, as we already demonstrated in the previous section, the reactivity of the system is mainly concentrated around the transition metal, and so the local reactivity indices are of greater interest given their dependence on $\vec{r}$. Consequently, the local reactivity will be described using the nucleophilic (f_M^-) and electrophilic (f_M^+) Fukui functions condensed around the metal atoms as well as the corresponding nucleophilic (s_M^-) and electrophilic (s_M^+) local softness. The resulting finite difference reactivity indices for single electron transfer are listed in Table 3.

According to Table 3, the electronegativity of the metal-supported systems shows an increasing trend throughout both periods and groups, in perfect analogy with the Mulliken electronegativity of the free metal atom (Table 2). This observation is again indicative of the fact that the reactivity of the active site of this catalyst is mainly influenced by the properties of the transition metal atom. The assumption that the overall system's reactivity is mainly associated with the transition metal is further confirmed by means of the dual descriptor, defined as the difference between the electrophilic and nucleophilic Fukui function [Eq. (8)]. Within the finite difference approach,

Table 3. Summary of the global and local reactivity indices obtained through a finite difference approach with full electron transfer.

	$\Delta N = \pm 1$ electron					
	$\chi_{M/S}$[a]	S[b]	f_M^+[c]	f_M^-[c]	s_M^+[d]	s_M^-[d]
Fe	2.20	0.29	0.16	0.23	0.05	0.07
Ru	2.36	0.29	0.23	0.33	0.07	0.10
Os	2.76	0.29	0.31	0.35	0.09	0.10
Co	2.44	0.25	0.13	0.29	0.03	0.07
Rh	2.99	0.26	0.30	0.30	0.08	0.08
Ir	3.00	0.26	0.35	0.38	0.09	0.10
Ni	2.60	0.24	0.04	0.24	0.01	0.06
Pd	2.70	0.16	0.08	0.26	0.01	0.04
Pt	2.80	0.16	0.11	0.27	0.02	0.04

[a] Mulliken electronegativity [eV]. [b] Global softness [eV^{-1}]. [c] Fukui functions [a.u.]. [d] Local softness [$a.u.eV^{-1}$].

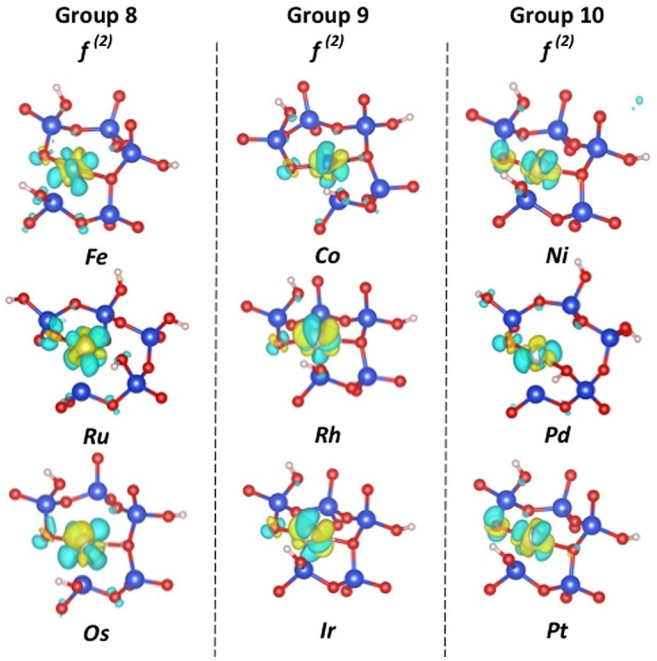

Figure 6. Graphical representation of the finite difference dual descriptor for silica-supported Group 8–10 d-transition metal atoms (isovalue = 0.005 a.u.).

the isosurfaces for the dual descriptor in Figure 6 clearly indicate that the region surrounding the d-transition metal is the most susceptible to accept or donate electrons. The specific shape of the dual descriptor suggests that electron acceptance/donation is primarily to/from the metal d-orbitals.

Therefore, in order to quantitatively describe the extent to which the active site is involved in a nucleophilic or electrophilic reaction, condensed finite difference Fukui functions for the addition and removal of a full electron were calculated based on Equation (7). The next sequence in increasing nucleophilic and electrophilic Fukui functions is obtained:

f^-: Ir > Os > Ru > Rh > Co > Pt > Pd > Ni > Fe

f^+: Ir > Os > Rh > Ru > Fe > Co > Pt > Pd > Ni

From this sequence it can be observed that both the nucleophilic and electrophilic Fukui functions tend to intensify as one moves down a group of the periodic table. Furthermore, the

reactivity of the catalytic particle appears to be proportional to the adsorption energy, as the most strongly adsorbed metal atoms are characterized by the highest Fukui values. Since the differences in global softness (*S*) compared to the Fukui functions are fairly small and these values are almost identical within the same group, it is not surprising that the local softness follows analogous reactivity trends as the Fukui functions. In view of the irreducible nature of the surface and the fact that the reactivity is located around the transition metal, one would, however, expect that the trends in local reactivity indices would strongly correlate with the chemical characteristics of the transition metals, which does not appear to be the case. For instance, the elements that oxidize most easily (Period 4 metals) should be associated with the highest nucleophilic Fukui functions. These inconsistencies can probably be attributed to the finite difference approximation, which, despite its frequent use for describing the reactivity of atoms and molecules, displays some shortcomings for periodic systems. As such, the introduction or withdrawal of an electron induces an artificial undesired Coulomb interaction between the charged cell and successive reciprocal cells due to its periodicity. Despite the introduction of a first-order term[60] that allows the total energy of the charged system to be corrected for background charge, Cardenas et al.[61] suggested that the influence of this electrostatic interaction is expected to be significant for systems with pronounced local density of states around the Fermi level, as appears to be the case for the described d-transition metals. A possible way to attenuate the influence of this interaction consists of using a fractional electron transfer in order to reduce the introduced charge. The obtained reactivity indices for $N\pm0.1$ and $N\pm0.01$ electron systems can be found in Table S2 (Supporting Information). These data show a general numerical increase in both global softness and local indices with decreasing fraction of charge transfer, while maintaining the already established trends for single electron transfer. Nevertheless, we conclude that determining reactivity indices by means of a finite difference approximation remains unsuitable for our silica-supported single-atom catalysts independently of the amount of considered electrons.

Evaluating the reactivity of silica-supported SACs through a density of states approach

An alternative approach that avoids the aforementioned shortcomings relies on the integration of the density of states. Within this scheme, the global softness (*S*) is defined as the inverse of the system's band gap, while the local indices are obtained by integrating the local density of states (LDOS) condensed on the supported metal atom between the Fermi level and an infinitesimal small bandwidth ($\delta\mu$). The introduction of such a bandwidth $\delta\mu$ brings into account the contribution of the discrete energy levels located around the Fermi level, defined as the point at which integration of the energy bands corresponds to the amount of electrons in the considered system, to the reactivity of the surface. In this respect, an integration over the valence band (negative $\delta\mu$ values) gives rise to a nucleophilic local index, while the integration with the Fermi level as a lower limit results into electrophilic indices. In order to minimize the influence of the chosen bandwidth on the calculated indices, the convergence of the nucleophilic Fukui function (f_M^-) was investigated for $\delta\mu$ values ranging from -0.05 to -1.00 eV. The corresponding convergence data, graphically represented for Group 8 elements in Figure 7, show that the nucleophilic Fukui function of a fourth period metal (Fe) appears to be independent of the considered bandwidth (for the full dataset, see Table S3(Supporting Information)). For the heavier elements, this local index remains constant for bandwidths ranging between -0.05 and -0.30 eV, after which a steady increase is observed. Consequently, it was decided to evaluate the nucleophilic local indices for the smallest possible $\delta\mu$ value of -0.05 eV.

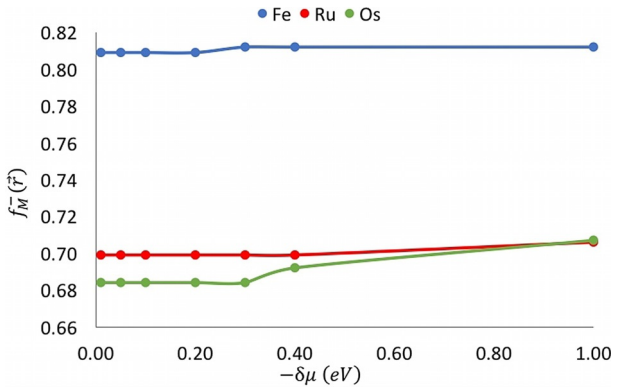

Figure 7. Nucleophilic Fukui function (f_M^-) evaluated at different $\delta\mu$ values for Fe (blue), Ru (red) and Os (green).

In the case of the electrophilic local indices, determining one specific $\delta\mu$ value allowing the description of all systems turned out to be much more complicated. This is due to the fact that the orbital contribution of the different metals to the system's conduction band is much less densely concentrated around the Fermi level, as can be observed from the density of states plots in Figure S3–S20 (Supporting Information). Consequently, integration of the DOS over small positive $\delta\mu$ ranges would correspond to an integration over a vacuum space. Therefore, the smallest possible $\delta\mu$ value within the first significant orbital contribution peak was used to determine the corresponding electrophilic Fukui function (f_M^+) and local softness (s_M^+) for each individual metal. The reactivity indices obtained from the density of states approach are summarized in Table 4.

The global softness, defined as the inverse of the band gap (Table 4), displays, in agreement with the finite difference approximation, a decreasing trend between elements originating from consecutive groups of the periodic table. Besides, a descending trend is also observed within groups, with the global softness for systems consisting of the fourth period elements being substantially higher than for the heavier metals. Furthermore, it is also noted that the differences in global softness between row 5 and 6 elements are considerably less pronounced. These observations are however in contradiction with the established trends in Mulliken electronegativity as well as chemical characteristics of the different d-metals. This is probably due to the improper description of band gaps with the PBE

Table 4. Summary of the global and local reactivity indices obtained through the density of states approach.

	DOS approach				
	$S^{[a]}$	$f_M^{+[b]}$	$f_M^{-[b]}$	$s_M^{+[c]}$	$s_M^{-[c]}$
Fe	1.01	0.80	0.81	0.81	0.82
Ru	0.49	0.75	0.70	0.37	0.34
Os	0.40	0.72	0.68	0.29	0.27
Co	0.87	0.83	0.84	0.72	0.73
Rh	0.47	0.71	0.73	0.33	0.34
Ir	0.39	0.71	0.74	0.28	0.29
Ni	0.67	0.48	0.81	0.32	0.54
Pd	0.37	0.40	0.69	0.15	0.26
Pt	0.39	0.42	0.60	0.16	0.23

[a] Global softness [eV^{-1}]. [b] Fukui functions [a.u.]. [c] Local softness [$a.u.\,eV^{-1}$].

and other GGA functionals. A quantitative and more detailed characterization of this reactivity index would require the use of a hybrid functional, but at the expense of a significant increase in computational cost. Alternatively, the introduction of a Hubbard term might also improve the description of the band gap and, consequently, of the global softness derived from it. However, this correction term appears to be highly dependent on both the considered system, property of interest and the computational parameters,[62] hence requiring a comprehensive benchmark prior to its implementation making it computationally more demanding as compared to the proposed methodology in this work.

Regarding the description of the nucleophilic Fukui functions, a significant change over the finite difference approximation method is perceived. As such, the condensed nucleophilic Fukui function (f_M^-), corresponding to the oxidation of the metallic center, is the largest for every row 4 element (Fe, Co, Ni) with a value fluctuating around 0.80 a.u. (Table 4). This finding is fully in line with the slightly negative reduction potentials associated with the conversion of the metallic ion to the corresponding uncharged particle,[63] supporting the preference for the oxidized state or high nucleophilic Fukui function. Furthermore, this observation can also be correlated with the smaller Mulliken electronegativity as compared to the heavier elements, corresponding to a weaker attraction of electrons. The distinctly lower, but analogous chemical behavior of the active sites consisting of a transition metal originating from the fifth or sixth period is fully in line with the known limited reactivity of these platinum group elements under normal chemical conditions.[64] Despite the promising correlation between the calculated condensed nucleophilic Fukui functions and the chemical properties of the considered transition metals, it turns out that the electrophilic local indices of the adsorbed Group 8 and 9 metals are much harder to connect with their characteristics. It can actually be noted from Table 4 that the electrophilic Fukui functions of these systems are characterized by very similar values as the nucleophilic index, whereas given the small Bader charges the active site of these catalysts are presumed to have more atomic than ionic behavior. Therefore, these metals are expected to behave as electron donors rather than acceptors corresponding to a low electrophilic reactivity index.

Consequently, further improvements towards a more robust way to determine reactivity indices for periodic systems are required. In this regard, Zhuang et al.[49] introduced a weighted density of states approach in which the weight factor corresponds to the derivative of the Fermi-Dirac distribution function at temperatures different from zero. This approach is considered a further refinement of the classical density of states approach outlined in Equation (10), as it takes into account that not every state around the Fermi level contributes equally to the reactivity. As mathematically derived in the Appendix, the resulting global (S_F) and local Fermi softness (s_F) is proven to be a very good approximation for the global (S) and local softness (s_M) when the relaxation term describing the influence of a changing chemical potential on the density of states is neglected. Subsequently, the condensed Fukui functions were obtained as the ratio of the local Fermi softness (s_F) to the global Fermi softness (S_F) by analogy with Equation (9), in which case a distinction between nucleophilic and electrophilic reactivity indices also needs to be established. Since the initial density of states approach indicated a reasonable constant feature for the nucleophilic Fukui function within a bandwidth of −0.30 eV (Figure 7), the weight function was chosen such that each state within this range was assigned a weight factor of at least 0.1 %. The reactivity indices obtained for a weight function described by a nominal electron temperature kT of 0.10 eV can be found in Table 5.

Table 5. Summary of the global and local reactivity indices obtained through the weighted density of states approach.

	Weighted DOS approach				
	$S_F^{[a]}$	$f_M^{+[b]}$	$f_M^{-[b]}$	$s_M^{+[c]}$	$s_M^{-[c]]}$
Fe	2.86	0.002	0.81	0.006	2.32
Ru	2.25	0.044	0.66	0.098	1.49
Os	2.34	0.004	0.68	0.010	1.60
Co	2.37	0.041	0.80	0.097	1.89
Rh	2.31	0.007	0.70	0.016	1.61
Ir	2.45	0.001	0.73	0.003	1.78
Ni	6.80	0.000	0.82	0.000	5.57
Pd	4.63	0.000	0.68	0.000	3.14
Pt	4.67	0.000	0.62	0.000	2.88

[a] Global Fermi softness [eV^{-1}]. [b] Fukui functions [a.u.]. [c] Local Fermi softness [$a.u.\,eV^{-1}$].

This table reveals that the numerical values obtained for the global Fermi softness are significantly higher than those obtained for the global softness by means of the classical density of states approach. In this respect, it should be noted that the silica adsorbed Group 10 systems with fully filled valence band are characterized by the largest values. In addition, the Fermi softness for the adsorbed platinum group elements (Ru, Os, Rh, Ir, Pd and Pt) shows an increasing trend throughout successive periods and groups. The higher tendency towards charge transfer of systems consisting of a row 6 element instead of a row 5 transition metal is probably related to their

enhanced Mulliken electronegativity, while differences in electronic configuration between successive groups might explain the higher Fermi softness of for example a silica adsorbed iridium system (2.45 eV^{-1}) with respect to osmium (2.34 eV^{-1}). As such, the former system is characterized by a doublet multiplicity corresponding to a configuration that lacks only one electron to obtain a fully filled valence band, whereas a Group 8 system consists of an incompletely filled electron shell in which two unpaired electrons reside. It therefore seems plausible that the system consisting of a Group 9 transition metal will strive to acquire a close-shell configuration and is hence more inclined to undergo a charge transfer process. The previous discussion, however, does not appear to be fully consistent for the period 4 elements, as especially Fe (2.86 eV^{-1}) and to a lesser extent Co (2.37 eV^{-1}) show a higher Fermi softness despite their lower electronegativity. We hypothesize that the more pronounced tendency of these systems for an oxidized metallic state is the driving force towards an easy charge transfer from the catalyst to the reactant, and hence a higher softness value.

Additionally, the introduction of weight factors appears to have very little influence on the quantitative determination of the nucleophilic Fukui functions and hence reinforces the previously described correlation between this reactivity index and the small negative reduction potentials of row 4 elements on the one hand and the rather inert character of the remaining transition metals on the other hand. However, in contrast to the classical density of states approach, a clear difference between the electrophilic and nucleophilic Fukui functions is revealed. As such, all considered transition metals, regardless of their location in the periodic table, are described by an f_M^+ function that is nearly equal to zero, whereas in the classical DOS approach the electrophilic Fukui function displayed almost identical values as the nucleophilic one. These extremely low values are, nevertheless, in better agreement with the observation that the conduction band is much less densely concentrated around the Fermi level, therefore limiting the amount of energy states that contribute to the reactivity. Furthermore, this also supports our assumption that the silica-adsorbed late transition metals exhibit little reducible character. The local Fermi softness for all silica-adsorbed d-metals, except for Pd and Pt, shows very similar trends as the corresponding Fukui functions, indicating that the transition metals with a higher propensity to undergo charge transfer reactions are also more prone to accommodate the respective charge.

The determination of a suitable catalyst for a chemical reaction on an experimental scale is, however, not only determined by the observed reactivity of the active species but is also influenced by the selectivity of these species for a given end product as well as reaction conditions such as temperature, pressure or acidic medium. Nevertheless, our findings appear to be consistent with the recent experimental observations regarding the use of catalysts for the Sabatier reaction. Accordingly, the electrocatalytic conversion of CO_2 into CO appears to proceed very easily in the presence of catalysts containing metal atoms of the fourth period at low overpotential.[65] Moreover, the difference in turn-over frequencies between these metal atoms appears to be very small, by analogy with their almost identical values for the nucleophilic Fukui function (f_M^-). Additionally, the effect of temperature on the activity of Pd-, Ni- and Rh-based catalysts in conversion of CO_2 into CO was studied showing a steep increase in conversion for the Ni-based catalyst and a moderate enhancement for Rh and Pd.[66] The distinctly less pronounced difference in activity between Pd and Rh with respect to that of Rh and Ni is also consistent with the observed decrease in Fukui functions within the order Ni (0.82) $\gg$ Rh (0.70) $>$ Pd (0.68). Given the consistency between our computational findings and the results of the abovementioned experimental studies, we believe that the proposed systematic analysis of such catalysts by means of conceptual DFT indices can generate alternative insights for further development in the field of single atom catalysis.

Conclusions

The role of the various parameters in the adsorption of a single late transition metal atom on an amorphous silica surface with a hydroxylation degree of 5.8 $OH^- nm^{-2}$ was rationalized by using periodic DFT. This investigation shows that the strength of the adsorption is highly dependent on the nature of the metal atom as well as different binding sites of the amorphous silica surface with adsorption energies ranging from 0.91 to -2.92 eV. The weakest metal–silica interactions obtained for the inert Ag or Au metal atom surrounded by a maximum number of stabilizing hydroxy groups were found to be mainly driven by van der Waals dispersion forces. In contrast to Ag and Au, transition metals from Group 8, 9 and 10 as well as Cu seem to interact preferentially with binding sites consisting of larger silica ring systems and low hydroxylation degree despite their rather diverging binding affinities. The strength of their interaction with the amorphous silica support appears to be affected by the oxophilicity of the transition metal. Accordingly, it was observed that metal atoms of row 4 (Fe, Co, Ni), which are more prone to transfer electrons to the surface given their smaller electronegativity, are characterized by larger Bader charges at the expense of a decrease in the adsorption energies (E_{ads} in the range of -1.40 to -1.92 eV). With the exception of the Pd atom, the heavier row 5 and 6 metals, with a less pronounced tendency to electron transfer, are associated with stronger adsorption energies varying between -2.20 and -2.92 eV. This direct relationship between the electronegativity of the transition metal atom and the adsorption energy is a clear indication that the considered silica surface retains its irreducible character even after adsorption. The relatively weak interaction of the Pd atom with the silica surface ($E_{ads} = -1.21$ eV) can probably be attributed to its fully filled d-shell. This implies that, unlike other Group 8–10 transition metals, no stabilizing hybridization effects allowing the transfer of s-electrons of the transition metal into incompletely filled d-orbitals can occur. From our analysis of both the bonding distances and density of states it appears that the interaction of the different Group 8–10 transition metal atoms with the silica surface involves the formation of covalent M–O and M–Si bonds upon breaking of a Si–O bond. Moreover, it can also be

hypothesized that an additional donor–acceptor interaction between the metal and the lone pair of the neighboring oxygen atom further stabilizes the formed catalytic complex.

Subsequently, the reactivity of these supported single-atom catalytic systems (Group 8–10) was evaluated by using three different theoretical schemes, introduced in a particular order reflecting the gradual improvement in the obtained values. The finite difference approximation, which is commonly used for the reactivity of molecules, was found to be unsuitable for an accurate description of the periodic models as it probably suffers from an artificial Coulomb interaction between consecutive reciprocal cells due to the introduction of charged species. The absence of charges in the classic density of states approach ensures a slight improvement in terms of local reactivity, yet this method proves not to be the most robust as it appears to be dependent on the DFT functional used. The introduction of a weight function, in the case of the Fermi weighted density of states approach, provides a more accurate description of the reactivity with respect to the classic DOS approach, as it enabled the fact that that the energy states nearest to the Fermi level affect the final reactivity of the considered catalytic particle more than the low-lying ones to be taken into account. In addition, this weight function makes this approach less sensitive to the accuracy of the description of band gaps with GGA functionals. Consequently, we conclude that the most reliable values of the cDFT reactivity descriptors for periodic systems are obtained when using the Fermi-weighted DOS approach. The reactivity indices obtained from this approach correlate well with the characteristics of the considered metals as well as experimental findings. In this regard, all investigated systems are classified by a distinct soft character, with a further enhancement of the Fermi softness as the electronegativity or filling of the valence band increases. Furthermore, the obtained values for the nucleophilic Fukui functions (f_M^-) were significantly higher than those for the electrophilic Fukui functions (f_M^+); this is consistent with the preferential electron-donating rather than -accepting character of the late transition metals. Additionally, the highest values for the nucleophilic Fukui function ($f_M^- \approx$ 0.80 a.u.) were found for systems consisting of adsorbed row 4 elements characterized by slightly negative standard reduction potentials and hence expressing a preference for their oxidized state. The chemically similar and reasonably inert remaining platinum group metals appear to be characterized by comparable Fukui functions, lower than those for the other considered metals. In summary, our results indicate that the conceptual DFT reactivity descriptors reflect the features of the catalytic active site and may consequently be applied as a valuable tool for the interpretation of the experimental catalytic data.

Appendix: local softness for periodic systems

In this appendix, we summarize the different equations to obtain the softness and local softness from the band structure of periodic systems. For a periodic system, the number of electrons N is given as [Eq. (12)]:

$$N = \int_{-\infty}^{+\infty} g(\varepsilon) f(\varepsilon) d\varepsilon \tag{12}$$

with μ the chemical potential, $g(\varepsilon)$ the density of states, T the temperature and $f(\varepsilon)$ the Fermi-Dirac distribution function [Eq. (13)]:

$$f(\varepsilon) = \frac{1}{e^{\frac{(\varepsilon-\mu)}{kT}} + 1} \tag{13}$$

The global softness S is defined as:

$$S = \left(\frac{\partial N}{\partial \mu}\right)_v \tag{14}$$

where v is the external potential. Using Eq. (12), the global softness becomes:

$$S = \frac{\partial}{\partial \mu}\left[\int_{-\infty}^{+\infty} g(\varepsilon) f(\varepsilon) d\varepsilon\right]_v = \int_{-\infty}^{+\infty} \left(\frac{\partial [g(\varepsilon) f(\varepsilon)]}{\partial \mu}\right)_v d\varepsilon \tag{15}$$

Or:

$$S = \int_{-\infty}^{+\infty} \left(\frac{\partial g(\varepsilon)}{\partial \mu}\right)_v f(\varepsilon) d\varepsilon + \int_{-\infty}^{+\infty} g(\varepsilon) \left(\frac{\partial f(\varepsilon)}{\partial \mu}\right)_v d\varepsilon \tag{16}$$

At $T=0$:

$$\left(\frac{\partial f(\varepsilon)}{\partial \mu}\right)_v = \delta(\varepsilon - \mu) \tag{17}$$

Thus, again at $T=0$, one obtains, taking into account that at $T=0$, $g(\varepsilon) = 0, \forall \varepsilon > \mu$:

$$S = g(\mu) + \int_{-\infty}^{\mu} \left(\frac{\partial g(\varepsilon)}{\partial \mu}\right)_v d\varepsilon \tag{18}$$

If the second (relaxation) term is neglected, i.e. assuming that $g(\varepsilon)$ only slowly varies with μ we find that:

$$S \approx g(\mu) \tag{19}$$

i.e. the global softness is the density of states at the Fermi level.[43]

At $T>0$, the global softness S becomes:

$$S = \int_{-\infty}^{+\infty} \left(\frac{\partial g(\varepsilon)}{\partial \mu}\right)_v f(\varepsilon) d\varepsilon + S_F \tag{20}$$

The last term in this equation is the so-called Fermi softness S_F, introduced by Zhuang et. al.[49]

Again assuming that $g(\varepsilon)$ does not depend on μ, one finds that $S = S_F$, i.e. the Fermi softness is equal to the finite temperature softness.

The same analysis can be done for the local softness $s(\vec{r})$.[43,61]

The local softness is defined as:

$$s(\vec{r}) = \left(\frac{\partial \rho(\vec{r})}{\partial \mu}\right)_v \tag{21}$$

The electron density $\rho(\vec{r})$ is expressed as:

$$\rho(\vec{r}) = \int_{-\infty}^{+\infty} g(\varepsilon,\vec{r}) f(\varepsilon) d\varepsilon \tag{22}$$

with $g(\varepsilon,\vec{r})$ the local density of states.

At $T=0$, one now proves, again assuming that the derivative of the local density of states with respect to the chemical potential is zero, that:

$$s(\vec{r}) \approx g(\mu,\vec{r}) \tag{23}$$

, i.e. the local softness is the local density of states at the Fermi level.[43]

In practise, the local softness can be computed as:[45,46,48]

$$s(r) = \lim_{\Delta\mu\to 0} \frac{\Delta}{\Delta\mu}\left[\int_0^{\mu+\Delta\mu} g(\varepsilon,\vec{r})d\varepsilon - \int_0^{\mu} g(\varepsilon,\vec{r})d\varepsilon\right]_v = \lim_{\Delta\mu\to 0} \frac{\Delta}{\Delta\mu}\left[\int_{\mu}^{\mu+\Delta\mu} g(\varepsilon,\vec{r})d\varepsilon\right]_v \tag{24}$$

At $T>0$, again neglecting the relaxation term, one obtains:

$$s(\vec{r}) \approx S_F(\vec{r}) \tag{25}$$

One can then use $S_F(\vec{r})$ as a reactivity index; we postulate, in analogy with the situation of the local softness at zero temperature, that integrating up to the chemical potential would model an electrophilic attack, integrating from the chemical potential upwards would describe a nucleophilic attack. The idea is basically to consider the local density around the Fermi level at T and to introduce a weight function that is peaked around this level:

$$S_F^-(\vec{r}) = \int_{-\infty}^{\mu} g(\varepsilon,\vec{r})\left(\frac{\partial f(\varepsilon)}{\partial\mu}\right)_v d\varepsilon \tag{26}$$

for an electrophilic attack and :

$$S_F^+(\vec{r}) = \int_{\mu}^{+\infty} g(\varepsilon,\vec{r})\left(\frac{\partial f(\varepsilon)}{\partial\mu}\right)_v d\varepsilon \tag{27}$$

for a nucleophilic attack.

Acknowledgements

The authors wish to thank the Vrije Universiteit Brussel (VUB) for the continuous support. F.D.P. acknowledges the VUB for a Strategic Research Program and the Francqui Foundation for a position as Francqui research professor. M.A. and J.T. would like to acknowledge the financial support of the Research Foundation-Flanders (projects no. 12F4416N and 12Y7718N). Computational resources and services were provided by the Shared ICT Services Centre funded by the Vrije Universiteit Brussel, the Flemish Supercomputer Centre (VSC) and FWO. P.W.A. acknowledges support from NSERC, the Canada Research Chairs, Canarie and Compute Canada.

Conflict of Interests

The authors declare no conflict of interests.

Keywords: amorphous silica · density functional calculations · reactivity indices · single-atom catalysis · transition metals

[1] a) X.-F. Yang, A. Wang, B. Qiao, J. Li, J. Liu, T. Zhang, *Acc. Chem. Res.* **2013**, *46*, 1740; b) J. Liu, *ACS Catal.* **2017**, *7*, 34; c) L. Liu, A. Corma, *Chem. Rev.* **2018**, *118*, 4981; d) A. Wang, J. Li, T. Zhang, *Nat. Rev. Chem.* **2018**, *2*, 65; e) H. Zhang, G. Liu, L. Shi, J. Ye, *Adv. Energy Mater.* **2018**, *8*, 1701343; f) F. Chen, X. Jiang, L. Zhang, R. Lang, B. Qiao, *Chinese J. Catal.* **2018**, *39*, 893, and references therein.
[2] S. J. Tauster, *Acc. Chem. Res.* **1987**, *20*, 389.
[3] M. Yang, S. Li, Y. Wang, J. A. Herron, Y. Xu, L. F. Allard, S. Lee, J. Huang, M. Mavrikakis, M. Flytzani-Stephanopoulos, *Science* **2014**, *346*, 1498.
[4] J. C. Matsubu, V. N. Yang, P. Christopher, *J. Am. Chem. Soc.* **2015**, *137*, 3076.
[5] M. J. Kale, P. Christopher, *ACS Catal.* **2016**, *6*, 5599.
[6] J. Jones, H. Xiong, A. T. DeLaRiva, E. J. Peterson, H. Pham, S. R. Challa, G. Qi, S. Oh, M. H. Wiebenga, X. I. P. Hernandez, Y. Wang, A. K. Datye, *Science* **2016**, *353*, 150.
[7] Q. Feng, S. Zhao, Y. Wang, J. Dong, W. Chen, D. He, D. Wang, J. Yang, Y. Zhu, H. Zhu, L. Gu, Z. Li, Y. Liu, R. Yu, J. Li, Y. Li, *J. Am. Chem. Soc.* **2017**, *139*, 7294.
[8] Z. Chen, E. Vorobyeva, S. Mitchell, E. Fako, M. A. Ortuno, N. Lopez, S. M. Collins, P. A. Midgley, S. Richard, G. Vile, J. Perez-Ramirez, *Nat. Nanotechnol.* **2018**, *13*, 702.
[9] a) S. Fernandez, A. Markovits, F. Fuster, C. Minot, *J. Phys. Chem. C* **2007**, *111*, 6781; b) S. Fernandez, A. Markovits, C. Minot, *Chem. Phys. Lett.* **2008**, *463*, 106; c) S. Fernandez, A. Markovits, C. Minot, *J. Phys. Chem. C* **2008**, *112*, 16491.
[10] B. He, J. Shen, D. Ma, J. Wang, S. Cheng, Z. Tian, *Appl. Surf. Sci.* **2018**, *462*, 399.
[11] Y. Wang, X. Zhang, C. Cheng, Z. Yang, *Appl. Surf. Sci.* **2018**, *453*, 159.
[12] L. Qin, Y.-Q. Cui, T.-L. Deng, F.-H. Wei, X.-F. Zhang, *ChemPhysChem* **2018**, *19*, 3346.
[13] Y. Feng, Q. Wang, H. Xiong, S. Zhou, X. Chen, X. I. P. Hernandez, Y. Wang, S. Lin, A. K. Datye, H. Guo, *J. Phys. Chem. C* **2018**, *122*, 22460.
[14] X. Chen, X. Zhao, Z. Kong, W.-J. Ong, N. Li, *J. Mater. Chem. A* **2018**, *6*, 21941.
[15] M. Zhao, R. Zhao, W. Li, T. Wang, Y. Ma, X. Dai, *Appl. Surf. Sci.* **2019**, *471*, 678.
[16] H. Jing, Q. Li, J. Wang, D. Liu, K. Wu, *J. Phys. Chem. C* **2019**, *123*, 1235.
[17] J. Ma, H. Gong, T. Zhang, H. Yu, R. Zhang, Z. Liu, G. Yang, H. Sun, S. Tang, Y. Qiu, *Appl. Surf. Sci.* **2019**, *488*, 1.
[18] Q. Fu, T. Wagner, *Surf. Sci. Rep.* **2007**, *62*, 431.
[19] a) J. H. den Otter, S. R. Nijveld, K. P. de Jong, *ACS Catal.* **2016**, *6*, 1616; b) C. Vogt, E. Groeneveld, G. Kamsma, M. Nachtegaal, L. Lu, C. J. Kiely, P. H. Berben, F. Meirer, B. M. Weckhuysen, *Nat. Catal.* **2018**, *1*, 127; c) T. A. Le, J. K. Kang, E. D. Park, *Appl. Catal. A* **2019**, *581*, 67; d) Y. Park, Y. You, J. Han, T.-S. Kwon, C.-H. Lee, J.-K. Jeon, *J. Nanosci. Nanotechnol.* **2019**, *19*, 6412; e) H. Du, X. Ma, P. Yan, M. Jiang, Z. Zhao, Z. C. Zhang, *Fuel Process. Technol.* **2019**, *193*, 221.
[20] a) I. Yudanov, G. Pacchioni, K. Neyman, N. Rösch, *J. Phys. Chem. B* **1997**, *101*, 2786; b) A. Markovits, M. K. Skalli, C. Minot, G. Pacchioni, N. Lopez, F. Illas, *J. Chem. Phys.* **2001**, *115*, 8172; c) A. Markovits, J. C. Paniagua, N. Lopez, C. Minot, F. Illas, *Phys. Rev. B* **2003**, *67*, 115417.
[21] P. Schlexer, G. Pacchioni, *Top. Catal.* **2017**, *60*, 459.
[22] a) L. Xiao, W. F. Schneider, *Surf. Sci.* **2008**, *602*, 3445; b) C. K. Narula, G. M. Stocks, *J. Phys. Chem. C* **2012**, *116*, 5628.
[23] Z. Helali, A. Markovits, C. Minot, M. Abderrabba, *Struct. Chem.* **2012**, *23*, 1309.
[24] A. Figueroba, G. Kovacs, A. Bruix, K. M. Neyman, *Catal. Sci. Technol.* **2016**, *6*, 6806.
[25] a) B. Pinter, N. Nagels, W. A. Herrebout, F. De Proft, *Chem. Eur. J.* **2013**, *19*, 519; b) F. De Vleeschouwer, M. Denayer, B. Pinter, P. Geerlings, F. De Proft, *J. Comput. Chem.* **2018**, *39*, 557; c) M. Kohagen, F. Uhlig, J. Smiatek, *Int. J. Quantum Chem.* **2019**, *119*, e25933; d) Y. G. Wang, E. C. Barnes, S. Kaya, V. Sharma, *J. Comput. Chem.* **2019**, *40*, 2761; e) T. Bettens, M. Alonso, F. De Proft, T. A. Hamlin, F. M. Bickelhaupt, *Chem. Eur. J.* **2020**, *26*, 3884.

[26] a) F. Tielens, C. Gervais, J. F. Lambert, F. Mauri, D. Costa, *Chem. Mater.* **2008**, *20*, 3336; b) M. M. Islam, D. Costa, Calatayud, M. F. Tielens, *J. Phys. Chem. C* **2009**, *113*, 10740; c) H. Guesmi, R. Grybos, J. Handzlik, F. Tielens, *RCS Adv.* **2016**, *6*, 39424; d) M. Gierada, P. Michorczyk, F. Tielens, J. Handzlik, *J. Catal.* **2016**, *340*, 122; e) M. Gierada, J. Handzlik, *J. Catal.* **2018**, *359*, 261; f) M. Gierada, F. De Proft, M. Sulpizi, F. Tielens, *J. Phys. Chem. C* **2019**, *123*, 17343.
[27] a) G. Kresse, J. Hafner, *Phys. Rev. B* **1993**, *47*, 558; b) G. Kresse, J. Hafner, *Phys. Rev. B* **1994**, *49*, 14251; c) G. Kresse, J. Furthmuller, *Comput. Mater. Sci.* **1996**, *6*, 15; d) G. Kresse, J. Furthmuller, *Phys. Rev. B* **1996**, *54*, 11169.
[28] a) J. P. Perdew, K. Burke, M. Ernzerhof, *Phys. Rev. Lett.* **1996**, *77*, 3865; b) J. P. Perdew, K. Burke, M. Ernzerhof, *Phys. Rev. Lett.* **1997**, *78*, 1396.
[29] a) S. Grimme, J. Antony, S. Ehrlich, H. Krieg, *J. Chem. Phys.* **2010**, *132*, 154104; b) S. Grimme, S. Ehrlich, L. Goerigk, *J. Comput. Chem.* **2011**, *32*, 1456.
[30] a) P. E. Blöchl, *Phys. Rev. B* **1994**, *50*, 17953; b) G. Kresse, D. Joubert, *Phys. Rev. B* **1999**, *59*, 1758.
[31] H. J. Monkhorst, J. D. Pack, *Phys. Rev. B* **1976**, *13*, 5188.
[32] a) G. Henkelman, A. Arnaldsson, H. Jonsson, *Comput. Mater. Sci.* **2006**, *36*, 354; b) E. Sanville, S. D. Kenny, R. Smith, G. Henkelman, *J. Comput. Chem.* **2007**, *28*, 899; c) W. Tang, E. Sanville, G. Henkelman, *J. Phys. Condens. Matter* **2009**, *21*, 084204.
[33] a) R. G. Parr, W. T. Yang, *Annu. Rev. Phys. Chem.* **1995**, *46*, 701; b) H. Chermette, *J. Comput. Chem.* **1999**, *20*, 129; c) P. Geerlings, F. De Proft, W. Langenaeker, *Chem. Rev.* **2003**, *103*, 1793; d) L. Shu-Bin, *Acta Phys.-Chim. Sin.* **2009**, *25*, 590.
[34] a) P. Senet, *J. Chem. Phys.* **1996**, *105*, 6471; b) P. Senet, *J. Chem. Phys.* **1997**, *107*, 2516; c) P. W. Ayers, R. G. Parr, *J. Am. Chem. Soc.* **2001**, *123*, 2007; d) P. W. Ayers, J. S. M. Anderson, L. J. Bartolotti, *Int. J. Quantum Chem.* **2005**, *101*, 520.
[35] R. G. Parr, R. A. Donnelly, M. Levy, W. E. Palke, *J. Chem. Phys.* **1978**, *68*, 3801.
[36] R. G. Parr, R. G. Pearson, *J. Am. Chem. Soc.* **1983**, *105*, 7512.
[37] R. G. Parr, L. J. Bartolotti, *J. Am. Chem. Soc.* **1982**, *104*, 3801.
[38] a) P. W. Ayers, *J. Chem. Phys.* **2008**, *128*, 184108; b) F. Heidar-Zadeh, R. A. Miranda-Quintana, T. Verstraelen, P. Bultinck, P. W. Ayers, *J. Chem. Theory Comput.* **2016**, *12*, 5777; c) M. Franco-Pérez, J. L. Gázquez, P. W. Ayers, A. Vela, *J. Chem. Theory Comput.* **2018**, *14*, 597.
[39] R. G. Parr, W. T. Yang, *J. Am. Chem. Soc.* **1984**, *106*, 4049.
[40] J. P. Perdew, R. G. Parr, M. Levy, J. L. Balduz, *Phys. Rev. Lett.* **1982**, *49*, 1691.
[41] C. Morell, A. Grand, A. Toro-Labbe, *J. Phys. Chem. A* **2005**, *109*, 205.
[42] P. Geerlings, F. De Proft, *Phys. Chem. Chem. Phys.* **2008**, *10*, 3028.
[43] W. T. Yang, R. G. Parr, *Proc. Natl. Acad. Sci. USA* **1985**, *82*, 6723.
[44] M. H. Cohen, M. V. Gandugliapirovano, J. Kudrnovsky, *J. Chem. Phys.* **1994**, *101*, 8988.
[45] a) J. C. Santos, E. Chamorro, R. Contreras, P. Fuentealba, *Chem. Phys. Lett.* **2004**, *383*, 612; b) J. C. Santos, R. Contreras, E. Chamorro, P. Fuentealba, *J. Chem. Phys.* **2002**, *116*, 4311.
[46] a) C. Cardenas, M. Munoz, J. Contreras, P. W. Ayers, T. Gomez, P. Fuentealba, *Acta Phys. Chim. Sin.* **2018**, *34*, 631; b) L. T. Nguyen, F. De Proft, M. C. Amat, G. Van Lier, P. W. Fowler, P. Geerlings, *J. Phys. Chem. A* **2003**, *107*, 6837.
[47] K. D. Brommer, M. Galvan, A. Dalpino, J. D. Joannopoulos, *Surf. Sci.* **1994**, *314*, 57.
[48] C. Cárdenas?, F. De Proft, E. Chamorro, P. Fuentealba, P. Geerlings, *J. Chem. Phys.* **2008**, *128*, 034708.
[49] B. Huang, L. Xiao, J. Lu, L. Zhuang, *Angew. Chem. Int. Ed.* **2016**, *55*, 6239; *Angew. Chem.* **2016**, *128*, 6347.
[50] a) H. V. Thang, G. Pacchioni, L. DeRita, P. Christopher, *J. Catal.* **2018**, *367*, 104; b) H. V. Thang, S. Tosoni, L. Fang, P. Bruijnincx, G. Pacchioni, *ChemCatChem* **2018**, *10*, 2634; c) H. V. Thang, G. Pacchioni, *J. Phys. Chem. C* **2019**, *123*, 7271; d) H. V. Thang, G. Pacchioni, *ChemCatChem* **2020**, *12*, 2595.
[51] N. C. Hernández, J. F. Sanz, *J. Phys. Chem. B* **2002**, *106*, 11495.
[52] E. Wigner, F. Seitz, *Phys. Rev.* **1933**, *43*, 804.
[53] E. Wigner, F. Seitz, *Phys. Rev.* **1934**, *46*, 509.
[54] *Atomic Structure and Crystallochemical Properties of the Elements, Handbook of Physicochemical Properties of the Elements*, 1st ed. (Ed.: G. V. Samsonov), IFI/ Plenum, New York, **1968**.
[55] R. G. Pearson, *Inorg. Chem.* **1988**, *27*, 734.
[56] B. Cordero, V. Gomez, A. E. Platero-Prats, M. Reves, J. Echeverria, E. Cremades, F. Barragan, S. Alvarez, *Dalton Trans.* **2008**, *21*, 2832.
[57] K. Momma, F. Izumi, *J. Appl. Crystallogr.* **2011**, *44*, 1272.
[58] A. M. Asaduzzaman, P. Krüger, *J. Phys. Chem. C* **2008**, *112*, 19616.
[59] a) K. P. Kepp, *Inorg. Chem.* **2016**, *55*, 9461; b) K. A. Moltved, K. P. Kepp, *J. Phys. Chem. C* **2019**, *123*, 18432.
[60] G. Makov, M. C. Payne, *Phys. Rev. B* **1995**, *51*, 4014.
[61] M. L. Cerón, T. Gomez, M. Calatayud, C. Cardenas, *J. Phys. Chem. A* **2020**, *124*, 2826.
[62] *The DFT + U: Approaches, Accuracy, and Applications, S. A. Tolba, K. M. Gameel, B. A. Ali, H. A. Almossalami, N. K. Allam in Density Functional Calculations: Recent Progresses of Theory and Application* (Ed.: G. Yang), Intechopen, **2018**.
[63] *Electrochemical Series, Handbook of Chemistry and Physics*, 75th ed. (Ed.: D. R. Lide), CRC Press, Boca Raton, **1995**.
[64] *Platinum Group Metals and Compounds, H. Renner, G. Schlamp, I. Kleinwächter, E. Drost, H. M. Lüschow, P. Tews, P. Panster, M. Diehl, P. Tews, P. Panster, M. Diehl, J. Lang, T. Kreuzer, A. Knödler, K. A. Starz, K. Dermann, J. Rothaut, R. Drieselmann, C. Peter, R. Schiele, Ullmann's Encyclopedia of Industrial Chemistry*, Wiley, New York, **2002**.
[65] C. Vogt, M. Monai, G. J. Kramer, B. M. Weckhuysen, *Nat. Catal.* **2019**, *2*, 188.
[66] a) N. M. Martin, P. Velin, M. Skoglundh, M. Bauer, P.-A. Carlsson, *Catal. Sci. Technol.* **2017**, *7*, 1086; b) N. M. Martin, F. Hemmingsson, X. Wang, L. R. Merte, U. Hejral, J. Gustafson, M. Skoglundh, D. M. Meira, A. C. Dippel, O. Gutowski, M. Bauer, P.-A. Carlsson, *Catal. Sci. Technol.* **2018**, *8*, 2686.

Manuscript received: October 21, 2020
Revised manuscript received: December 15, 2020
Accepted manuscript online: December 26, 2020
Version of record online: March 4, 2021